Inorganica Chimica Acta 412 (2014) 20–26

Contents lists available at ScienceDirect

Inorganica Chimica Acta

journal homepage: www.elsevier.com/locate/ica

Synthesis, structure, redox properties and DNA interaction studies on mononuclear iron(III) complexes with amidate ligand

Kaushik Ghosh *, Nidhi Tyagi, Pramod Kumar, Udai P. Singh

Department of Chemistry, Indian Institute of Technology Roorkee, Roorkee 247667, India

ARTICLE INFO

Article history:
Received 14 August 2013
Received in revised form 22 November 2013
Accepted 26 November 2013
Available online 10 December 2013

Keywords:
Amidate ligand
Iron complexes
Crystal structure
DNA interaction
Nuclease activity

ABSTRACT

A new family of mononuclear Fe(III) complexes [Fe(Pamp)(MeOH)Cl_2], **1** and [Fe(Pamp)$_2$](ClO_4), **2** were synthesized using designed tridentate ligand PampH having pyridine and amide nitrogen donors (PampH is N′-phenyl-N′-(pyridin-2-yl)picolinohydrazide) and H stands for dissociable proton). Both the complexes (**1** and **2**) were characterized by different spectroscopic studies and molecular structure of [Fe(Pamp)$_2$](ClO_4), **2** was determined by single crystal X-ray diffraction. Geometry around metal centre was described as distorted octahedral with two meridionally oriented $Pamp^-$ ligands. Electrochemical studies afforded $E_{1/2}$ values of Fe(III)/Fe(II) couple +0.065 V (for **1**) and −0.077 V (for **2**) versus Ag/AgCl electrode. DNA binding properties of these complexes were investigated and complex **1** exhibited nuclease activity. Mechanistic investigation revealed the possible participation of hydroxyl radical in nuclease activity which was supported by rhodamine B assay.

1. Introduction

There has been considerable current interest for the synthesis of metal based synthetic nuclease because of their applications in discovery of artificial DNA cleaving agents, DNA foot-printing and in medicinal chemistry [1–6]. Cis-platin and Fe-bleomycin are the established metal based anticancer drugs [7–9]. Cis-platin is having lot many side effects and researchers are interested to discover metal based anti cancer agents with biologically benign metal rather than toxic metal like platinum [10]. Among first row transition elements iron exhibit flexible range of coordination geometries, oxidation states, spin states and redox potential and hence, iron became one of the suitable metals for the synthesis of artificial nuclease [11–13]. Several iron complexes were reported as artificial nucleases, however, most of them are multinuclear [3,14–23] and very few of them are mononuclear [24–26]. Among mononuclear complexes most of them were reported with salen and salen related ligands [27–29]. On the other hand, Roelfes et al. and Mukherjee et al. reported synthetic DNA cleavage agent of mononuclear iron complex in which ligand was covalently attached to a DNA-binder arm or intercalator as imidazopyridine ring and 9-aminoacridine (also acts as photosensitizer) respectively [30–31]. Wong et al. also reported nuclease activity of mononuclear iron complexes with tripodal ligands [32]. It is now well known in the literature that the ligation of deprotonated amidate nitrogen(s) stabilizes the iron(III) centres due to their strong σ-donating abilities [33]. Coordination chemistry of iron-amidate group participate important role in biomolecules such as anti-tumor drug bleomycin [34] and enzyme nitrile hydratase [35–36]. Fe(III) complexes derived from such ligand(s) have been exploited now as DNA cleaving agents [37]. Mascharak and co-workers reported mononuclear iron complex mimicking the iron binding site of belomycine (by designing the ligand having amidate group) however DNA binding and nuclease activity of these complexes were not reported [38].

Recently, we have communicated the role of carboxamido nitrogen in superoxide scavenging activity and nuclease activity [39–40]. Herein, we report the synthesis and characterization of two mononuclear iron complexes [Fe(Pamp)(MeOH)Cl_2], **1** and [Fe(Pamp)$_2$](ClO_4), **2**, derived from the amidate ligand PampH (shown in Scheme 1). These complexes were characterized by spectroscopic and electrochemical studies. Molecular structure of complex **2** was determined by X-ray crystallography. DNA interaction and nuclease activity were examined. We also investigated the mechanism of nuclease activity.

2. Experimental

2.1. Materials

All the solvents used were reagent grade. Analytical grade reagents picolinic acid (Wilson Laboratories, Mumbai, India), dicyclohexylcarbodiimide (SRL, Mumbai, India), 1-hydroxybenzotriazol (Himedia Laboratories Pvt. Ltd., Mumbai, India), phenylhydrazine, (S. D. Fine, Mumbai, India) and 2-chloropyridine (Acros organics,

* Corresponding author. Tel.: +91 1332285547; fax: +91 1332 273560.
E-mail address: ghoshfcy@iitr.ernet.in (K. Ghosh).

0020-1693/$ - see front matter © 2013 Elsevier B.V. All rights reserved.
http://dx.doi.org/10.1016/j.ica.2013.11.034

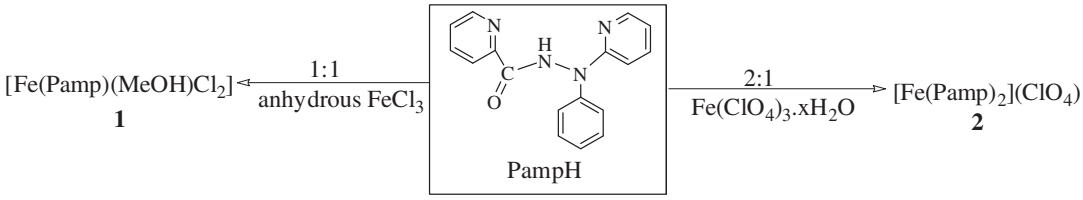

Scheme 1. Synthetic scheme of complex 1 and 2.

USA) were used as obtained. Anhydrous $FeCl_3$ was purchased from Rankem, Delhi, India and $Fe(ClO_4)_3{\cdot}xH_2O$, $Fe(ClO_4)_2{\cdot}xH_2O$, rhodamine B dye and 1,3-diphenylisobenzofuran (DPBF) were purchased from Sigma Aldrich, Steinheim, Germany. Solvent used for spectroscopic studies were HPLC grade and purified by standard procedure before use [41]. Supercoiled *pBR322* DNA and CT DNA were purchased from Bangalore Genei (India). Agarose was purchased from (Himedia Laboratories Pvt. Ltd., Mumbai, India). Tris(hydroxymethyl)aminomethane–HCl (Tris–HCl) buffer was prepared in deionised water.

Caution! Perchlorate salts of metal complexes with organic ligands are potentially explosive. Only small amount of material should be prepared and handled with caution.

2.2. Synthesis of complexes

2.2.1. [Fe(Pamp)(MeOH)Cl_2], **1**

A batch of (34 mg, 0.27 mmol) anhydrous $FeCl_3$ in 5 mL of methanol was added dropwise to stirred solution of ligand PampH (79.7 mg, 0.27 mmol) in 15 mL of methanol. The colour of solution was changed to dark green. The green solution was filtered to remove dirty suspension. Filtrate was again stirred for 3 h and the solution was kept in freeze for slow evaporation. Green colour semi-crystalline precipitate was obtained which was filtered and washed with small amount of methanol and diethylether. Though, complex **1** is precipitated as nice crystalline solid but all attempts to get single crystals were unsuccessful. Yield: 52.2 mg, (42%). Selected IR data (KBr, ν_{max}/cm^{-1}): 1658, 1603 $\nu_{-C=O}$. UV–Vis [CH_2Cl_2, λ_{max}/nm ($\varepsilon/M^{-1}cm^{-1}$)]: 626 (1450), 321 (9750), 248 (15,000). μ_{eff} (296 K): 5.19 BM. Λ_M/Ω^{-1} cm^2 mol^{-1} (in DMF): 12. *Anal.* Calc. for $C_{18}H_{17}N_4O_2Cl_2Fe$: C, 48.25; H, 3.82; N, 12.50. Found: C, 49.01; H, 3.67; N, 12.53%.

2.2.2. [Fe(Pamp)$_2$](ClO_4)

2.2.2.1. Method A. A batch of (50 mg, 0.14 mmol) $Fe(ClO_4)_3{\cdot}xH_2O$ in 5 mL of methanol was added dropwise, to the stirred solution of (80.7 mg, 0.28 mmol) ligand (PampH) in 10 mL of methanol. The colour of solution changed to red and then to brown. After 5 min, it turns to brownish-green solution which was stirred for 4 h. Dark green solid was separated out which was filtered and washed with methanol and small amount of diethylether. Single crystals of the complex for X-ray crystallography were obtained within a week on slow diffusion of acetonitrile/ethylacetate-diethyl ether mixture in freezer. Yield: 75.0 mg, (73%). Selected IR data (KBr, ν_{max}/cm^{-1}): 1602, $\nu_{-C=O}$, 1090, 622 ν_{ClO4-}. UV–Vis [CH_3CN, λ_{max}/nm (ε/M^{-1} cm^{-1})]: 801 (2000), 437 (3100), 315 (14,300), 251 (23,150). μ_{eff} (296 K): 2.75 BM, Λ_M/Ω^{-1} cm^2 mol^{-1} (in DMF): 58. *Anal.* Calc. for $C_{34}H_{26}N_8O_6ClFe$: C, 55.64; H, 3.57; N, 15.27. Found: C, 55.60; H, 3.72; N, 15.23%.

2.2.2.2. Method B. A batch of (30 mg, 0.12 mmol) $Fe(ClO_4)_2{\cdot}xH_2O$ in 5 mL of methanol was added dropwise, to the stirred solution of (72.5 mg, 0.25 mmol) ligand (PampH) in 10 mL of methanol. The colour of solution was changed to purple and within 1 min brownish-green solid was separated out. This green solid was filtered and washed with methanol and diethylether. Yield: 45 mg, (51%).

2.3. Physical measurements

Elemental analyses were carried microanalytically at Elemenlar Vario EL III. IR spectra were obtained as KBr pellets with Thermo Nikolet Nexus FT-IR spectrometer, using 16 scans and were reported in cm^{-1}. Electronic absorption spectra were recorded with an Evolution 600, Thermo Scientific UV–Vis spectrophotometer. Emission quenching titrations were carried out on Varian fluorescence spectrophotometer. Circular dichroism (CD) spectra of complexes (**1** and **2**) were recorded on Chirascan circular dichroism spectrometer, Applied photophysics, UK. Magnetic susceptibilities were determined at 296 K with Vibrating Sample Magnetometer model 155, using nickel as a standard. Diamagnetic corrections were carried out with Pascal's increments [42]. Molar conductivities were determined in dimethylformamide (DMF) at 10^{-3} M at 25 °C with a Systronics 304 conductometer. Cyclic voltammetry measurements were carried out using a CH-600 electroanalyzer. A conventional three-electrode arrangement was using consisting a platinum wire as auxiliary electrode, glassy carbon as working electrode and the Ag(s)/AgCl as reference electrode. These measurements were performed in the presence of 0.1 M tetrabutylammonium perchlorate (TBAP) as the supporting electrolyte, using complex concentration 10^{-3} M in dichloromethane and acetonitrile. The ferrocene/ferrocenium couple occurs at $E_{1/2}$ = +0.40 (75) V versus Ag/AgCl under the same experimental conditions. All experiments were performed at room temperature and solutions were thoroughly degassed with nitrogen prior to beginning the experiments.

2.4. X-ray crystal structure determination of complex **2**

Crystal and refinement data is given in Table 1. The X-ray data collection and processing for complex **2** was performed on Bruker Kappa Apex-II CCD diffractometer by using graphite monochromated Mo Ka radiation (k = 0.71070 Å) at 296 K. Crystal structure was solved by direct methods. Structure solution, refinement and data output was carried out with the SHELXTL program [43–44]. All non-hydrogen atoms were refined anisotropically. Hydrogen atoms were placed in geometrically calculated positions and refined using a riding model. Images were created with the DIAMOND program [45].

2.5. DNA binding experiments

Fluorescence quenching experiments were carried out by the successive addition of complexes **1** and **2** to the DNA (25 μM) solutions containing 5 μM ethidium bromide (EB) in 100 mM phosphate buffer (pH 7.2). For better solubility of complex **1** and **2**, we use 5% DMF. These samples were excited at 250 nm and emissions were observed between 500 and 700 nm. Stern–Vol-

Table 1
Summary of crystal data and data collection parameters for complex **2**.

Empirical formula	$C_{34}H_{26}N_8O_6ClFe$
Formula weight (g mol^{-1})	733.93
T (K)	296(2)
λ (Å) (Mo Kα)	0.71073
Crystal system	monoclinic
Space group	$P2_1/n$
a (Å)	11.1466(8)
b (Å)	9.2634(7)
c (Å)	30.935(2)
β (°)	91.306(3)
V (Å^3)	3193.4(4)
Z	4
ρ_{calc} (g cm^{-3})	1.527
Crystal size (mm)	0.25 × 0.17 × 0.11
$F(000)$	3280
θ Range for data collection	1.32–26.32
Index ranges	$-13 < h < 9$, $-9 < k < 11$, $-37 < l < 38$
Refinement method	full matrix least-squares on F^2
Data/restraints/parameters	6475/0/451
Goodness-of-fit (GOF) on F^2[a]	1.812
R_1[b] [$I > 2\sigma(I)$]	0.0722
R_1[all data]	0.0892
wR_2[c] [$I > 2\sigma(I)$]	0.2554
wR_2 [all data]	0.2641

[a] GOF = $[\sum[w(F_o^2 - F_c^2)^2]/(M-N)]^{1/2}$ (M = number of reflections, N = number of parameters refined).
[b] $R_1 = \sum||F_o| - |F_c||/\sum|F_o|$.
[c] $wR_2 = [\sum[w(F_o^2 - F_c^2)^2]/\sum[w(F_o^2)^2]]^{1/2}$.

mer quenching constants were calculated using the given equation,

$$I_0/I = 1 + K_{sv}Q,$$

Where I_0 and I are the fluorescence intensities in the absence and presence of complex and Q is the concentration of quencher (complexes **1** and **2**). K_{sv} is a linear Stern–Volmer constant and given by the ratio of slope to intercept in the plot of I_0/I versus Q [46].

Circular dichroism (CD) spectra of CT-DNA in absence and presence of the iron complexes were recorded with a 0.1 cm pathlength cuvette after 10 min incubation at 25 °C. The concentration of the complexes and CT-DNA were 50 and 200 μM respectively.

2.6. Nuclease activity

DNA cleavage was measured by the conversion of supercoiled *pBR322* plasmid DNA to nicked circular and linear DNA forms. Supercoiled *pBR322* DNA in (TBE) Trisboric acid-EDTA buffer (pH 8.2) was treated with complexes **1** and **2** taken in dimethylformamide (10%) in the presence or absence of additives. The oxidative DNA cleavage by the complexes were studies in the presence of H_2O_2 (oxidizing agent) and BME (reducing agent). The samples were incubated at 37 °C, added loading buffer (25% bromophenol blue and 30% glycerol). The agarose gel (0.8%) containing 0.4 ng/mL of ethidium bromide (EB) was prepared and the electrophoresis of the DNA cleavage products was performed on it. The gel was run at 60 V for 2 h in TBE buffer and the bands were identified by placing the stained gel under an illuminated UV lamp. The fragments were visualized by using a UV illuminator (BIO RAD).

2.7. Detection of reactive oxygen species (ROS)

The generation of reactive oxygen species (ROS) in the cleavage reaction was detected by dye degradation (rhodamine B) [47] or by using sensitive radical sensor (DPBF) [48]. Hydroxyl radical formation was quantified by 5 μM of rhodamine B in the presence of complexes **1**–**2** (0–300 μM) in MeOH under aerobic conditions. The degradation of the dye was monitored by the UV absorbance of rhodamine B at 544 nm. The fluorescent probes DPBF were used to detect the probable formation of $^1O_2$ during the nuclease reaction. Complexes 1 and 2 (0–100 μM) with DPBF (0.05 μM) in a methanol solution were used to monitor the changes in the fluorescence λ_{ex} = 405 nm, λ_{em} = 479 nm.

3. Results and discussion

3.1. Synthesis

The tridentate ligand PampH was synthesized and characterized by the reported procedure [39]. Ligand PampH when reacted with $FeCl_3$ in 1:1 equivalent ligand to metal ratio yielded green solid of $[Fe(Pamp)(MeOH)Cl_2]$, **1**. On the other hand, reaction of PampH with $Fe(ClO_4)_3{\cdot}xH_2O$ or $Fe(ClO_4)_2{\cdot}xH_2O$ in 2:1 (ligand to metal ratio) gave rise to $[Fe(Pamp)_2](ClO_4)$, **2**, in case of Fe(II) starting material we ended up with complex **2** due to aerial oxidation. Interestingly, during synthesis of **1** and **2** base was not needed for the deprotonation of PampH, the Lewis acidity of Fe(III) centre was efficient to deprotonate the ligand (PampH) [37]. The synthetic procedures of complexes **1** and **2** were described in Scheme 1.

3.2. Structure of complex *2*

The ORTEP diagram for cation of complex $[Fe(Pamp)_2]^+$, **2** is shown in Fig. 1. Matrix parameters, selected bond distances and bond angles are described in Table 1 and Table 2. Crystals of complex **2** were obtained from diethyl ether diffusion to a solution of **2** in acetonitrile-ethyl acetate (1:1) mixture at room temperature within a week. Complex **2** was crystallized in monoclinic space group $P2_1/n$ consisting of mononuclear iron(III) complex with six nitrogen atoms from two $Pamp^-$ ligands in distorted octahedral geometry. Complex **2** was isolated as the *mer* isomer with two carboxamido nitrogen (N2, N5) atoms occupying positions *trans* to each other however, all pyridine nitrogen donors (N1, N3, N4 and N6) were cis to each other. In complex **2**, the Fe–N_{am} bond lengths (1.884(4) Å and 1.890(4) Å) were consistent with reported values for complexes $[Fe(pmp)_2]^+$ (1.887(4) and 1.890(4) Å) [49] and $[Fe(bpc)(1\text{-MeIm})_2]^+$ (1.886 (4) Å, bpc = 4,5-dichloro-1,2-bis(pyridine-2-carboxamido)-benzene) [50] however, longer than in complex $[Fe(Pypep)_2](ClO_4)$ (1.957(2) and 1.958(2) Å) [38]. The average Fe–N_{py} distance (1.958 Å) in **2** was shorter than reported low-spin Fe(III) complexes 1.978 Å [37], 1.982 Å [38], 1.968 (3) Å [51] and 1.953(3) Å [52]. All the six Fe–N bonds have different bond lengths, the average Fe–N distance follows the order Fe–N_{am} (1.89 Å) < Fe–N_{Py} (1.95 Å). The appreciably shorter Fe–N_{am} bond was due to good donating properties of the amide nitrogen as well as the normal

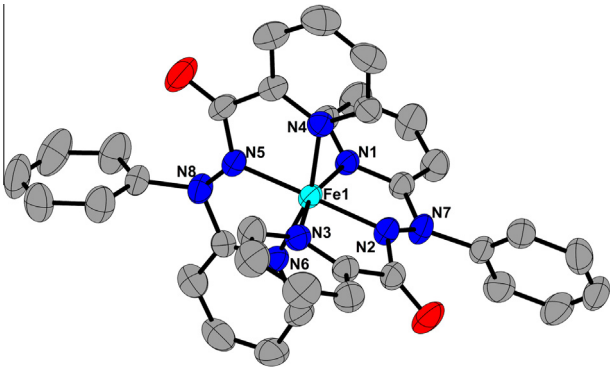

Fig. 1. ORTEP diagram (50% probability level) of complex $[Fe(Pamp)_2]^+$, **2**, hydrogen atoms were omitted for clarity.

Table 2
Selected bond lengths (Å) and angles (°) of complex **2**.

Bond distances (Å)		Bond angles (°)	
Fe1–N5	1.884(4)	N1–Fe1–N2	81.29(15)
Fe1–N2	1.890(4)	N2–Fe1–N3	81.62(16)
Fe1–N4	1.961(4)	N4–Fe1–N5	81.57(16)
Fe1–N6	1.946(4)	N5–Fe1–N6	81.33(16)
Fe1–N1	1.950(4)	N2–Fe1–N5	176.63(17)
Fe1–N3	1.975(4)	N4–Fe1–N6	162.79(16)
N2–N7	1.408(5)	N1–Fe1–N3	162.62(16)
N5–N8	1.396(5)	C13–C14–N3	114.0(4)
		C30–C29–N5	115.8(4)

tendency of tridentate ligands to have longer metal–ligand distances for the terminal bonds. The N–Fe–N angles showed maximum deviation from octahedral geometry with angles N2-Fe-N3 (81.62 (16)°), N1–Fe–N2 (81.29 (15)°), N4–Fe–N5 (81.57 (16)°) and N5–Fe–N6 (81.33(16)°). This was due to the short bite of the rigid pyridine-2-carboxamido moieties (five-membered chelate rings) all four N_{py}–Fe–N_{am} angles were ~81°, similar value was observed in $[M(bpca)_2]^+$ complexes [53–54]. Further support of strain in the five-membered chelate rings came from the C13–C14–N3 (114.0 (4)°) and C29–C30–N4 (115.82 (4)°) angles, which was away from the normal sp^2 angle of 120°.

3.3. Spectroscopic properties

Coordination of the deprotonated amido nitrogen to Fe(III) centre in **1** and **2** was expressed by the shift of $\nu_{C=O}$ from 1694 cm^{-1} in free ligand to 1657 and 1602 cm^{-1} for complexes **1** and **2** respectively. The decrease in $\nu_{C=O}$ frequency in both complexes clearly indicate the binding of deprotonated ligand (N_{am}) to the metal centre because partial double bond character in carbonyl moiety (shown in Scheme 2) is generated in C=O due to metal coordination. Similar, red shift of $\nu_{C=O}$ has been noted with other Fe(III) complexes having coordinated carboxamido nitrogens [38].

Deprotonation of amido nitrogens were further supported by disappearance of the band ν_{N-H} (3353 cm^{-1}) in IR spectra of metal complexes **1** and **2**. The presence of counter ion (ClO_4^-) in complex **2** was also confirmed by 1090 and 622 cm^{-1} bands. The IR spectra of both complexes were dominated by vibrations of the pyridyl rings as evidenced by the absorptions ~1465 and ~1555 cm^{-1} [55]. The UV–Vis spectra of complexes **1** and **2** were recorded in dichloromethane and acetonitrile respectively. For complex **1** the peak near 321 nm was assigned as chloro-to-Fe(III) charge transfer transition [56] and 248 nm was assigned as π–π^*, n–π^* transitions of ligand. Complex **1** also showed a broad band near 626 nm due to ligand-to-metal charge transfer transition (LMCT). Interestingly, for complex **2**, an absorption band near 800 nm assigned as ligand to metal charge transfer transition which was different than other low-spin Fe(III) complexes reported in literature [57]. The molar conductivities were determined in dimethylformamide at ca. 10^{-3} M at 25 °C. The values for **1** and **2** were 12.0 and 58.0 Ω^{-1}-cm^2 mol^{-1} respectively. These values for **1** and **2** were designated neutral and uni-univalent (1:1) electrolyte behaviour respectively [41,58]. Complex **1** showed a magnetic moment of 5.91 BM in the solid state at 296 K, suggesting a high-spin ($S = 5/2$) electronic configuration of iron(III). The effective magnetic moment value for complex **2** was 2.75 BM at 296 K supports the low-spin ($S = ½$) configuration in complex **2** [38].

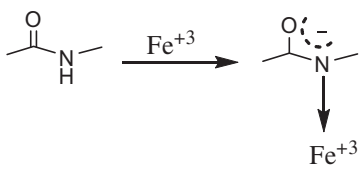

Scheme 2. Partial double bond character at carbonyl moiety.

3.4. Electrochemistry

Both complexes were electrochemically examined at a glassy carbon working electrode in acetonitrile (for **1**) and dichloromethane (for **2**) solutions. Representative cyclic voltammograms are displayed in Fig. 2 and reduction potentials are listed in Table 3. The redox processes were quasi-reversible ($\Delta Ep \sim 125$ mV) for both complexes (**1** and **2**) and exhibit a clean one electron-redox couple ($i_{Pa}/i_{Pc} \sim 1$). The half-wave potential ($E_{1/2}$) of the Fe(III)/Fe(II) couple of **1** was + 0.065 V (vs Ag/AgCl electrode) while **2** exhibit $E_{1/2}$ value of −0.077 V (vs Ag/AgCl electrode). The $E_{1/2}$ value of complex **1** was more positive side than reported literature (−0.040 V vresus Ag/AgCl) with one amidate ligand [59]. The $E_{1/2}$ value of complex **2** close to low-spin $[Fe(tacn)_2]^{3+}$ (−0.065 V versus Ag/AgCl) [60] however, very small as compared to $[Fe(Pypep)_2]^+$ (−0.235 V versus Ag/AgCl) [38]. Interestingly, the redox potential for Fe(III)/Fe(II) couple of **2** was observed at a more negative potential than that of **1** indicating stabilization of the Fe(III) species. The $E_{1/2}$ values of both complexes clearly designated that coordination of two amide nitrogens provide extra stability (due to strong σ donating capability) to the +3 oxidation state of low-spin Fe(III) in complex **2** as compared to high-spin Fe(III) complex **1**.

3.5. DNA interaction studies

We have investigated the DNA binding properties of complexes **1** and **2** by EtBr displacement assay via fluorescence spectrophotometer and circular dichroism spectral studies. We would like to mention here that complexes **1** and **2** in buffer did not show any characteristic peak by which we could study the titration with CT-DNA for the determination of binding constant to CT DNA. The Stern–Volmer quenching constant K_{SV} values (Fig. 3) for complexes **1** and **2** were 5.30×10^4 and 7.88×10^4 M^{-1} respectively, displayed poor binding propensity probably via external or surface binding to CT-DNA. Circular dichroic spectra of CT DNA exhibits a positive band at 275 nm due to base stacking, and a negative band at 245 nm due to the right handed helicity (Fig. S3 in Supporting information) [61]. On addition of complexes, the CD spectrum of

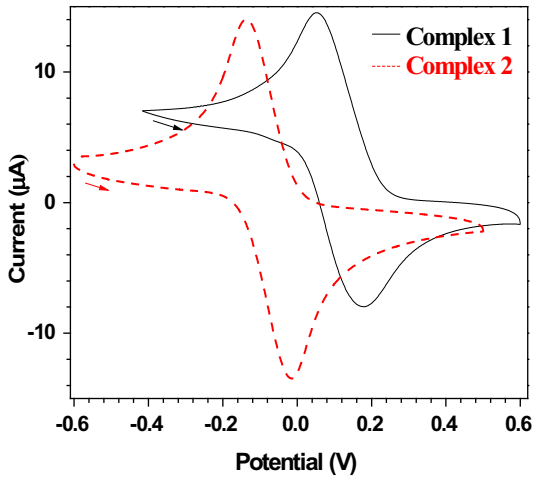

Fig. 2. Cyclic voltammograms of a 10^{-3} M solution of complexes **1** and **2**: using working electrode: glassy-carbon, reference electrode: Ag/AgCl; auxiliary electrode: platinum wire, scan rate 0.1 V/s.

Table 3
Cyclic voltammogram of complexes **1** and **2**.

Complex[a]	Fe(III)/Fe(II)			$n = i_{Pa}/i_{Pc}$[d]
	E_{pa}/V	E_{pc}/V	$E_{1/2}$[b], V (ΔE_p[c], mV)	
1	0.180	0.052	0.065 (128)	0.77
2	−0.016	−0.137	−0.077 (121)	1.00

[a] Measured in acetonitrile for **1** and in dichloromethane for **2** with 0.1 M tetrabutylammonium perchlorate (TBAP).
[b] Data from cyclic voltammetric measurements; $E_{1/2}$ is calculated as average of anodic (E_{pa}) and cathodic (E_{pc}) peak potentials $E_{1/2} = 1/2(E_{pa} + E_{pc})$.
[c] $\Delta E_p = E_{pa} - E_{pc}$ at scan rate 0.1 V/s.
[d] Constant-potential coulometric data $n = i_{pa}/i_{pc}$ calculated for $1e^-$ transfer.

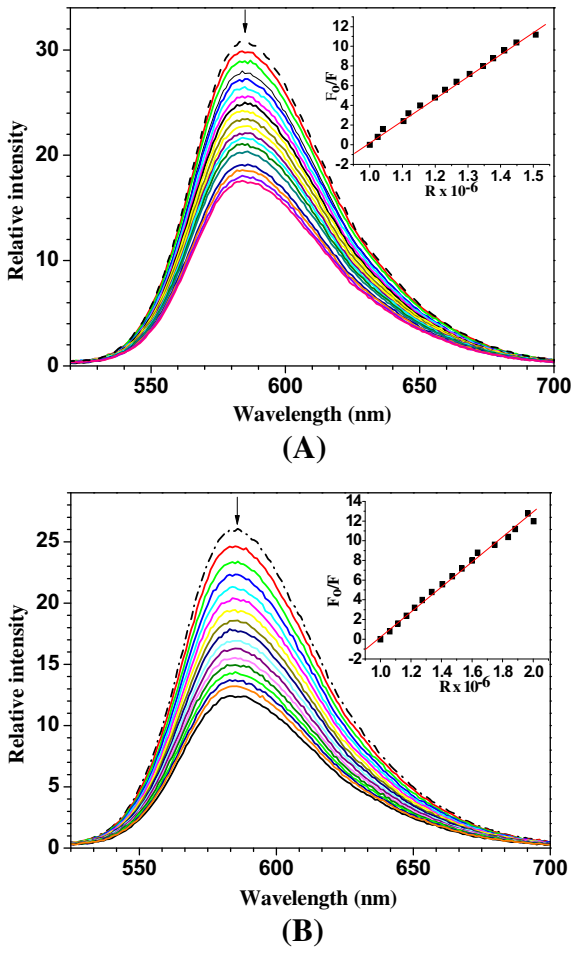

Fig. 3. EtBr–DNA fluorescence quenching titrations of using (A) complex **1** (0–38 μM), (B) complex **2** (0–34 μM), Stern–Volmer plots of F_o/F vs. [R] for both complexes shown in insets of respective graphs. Tests were performed in the conditions of 50 mM phosphate buffer (pH 7.2) at 298 K. C_{DNA} = 25 μM, C_{EtBr} = 0.5 - μM; λ_{ex} = 250 nm, λ_{em} = 602 nm.

DNA undergoes changes in both the positive and negative bands but no shift in the band positions. Considering the data obtained by fluorescence and circular dichroism spectral studies external interaction with CT-DNA was speculated [62].

3.6. Nuclease activity

The DNA cleavage behaviour of the complexes **1** and **2** were studied under physiological conditions (37 °C) and observed by the transformation of supercoiled form (SC or D_I) to the nicked (NC or D_{II}) and linear (LC or D_{III}) forms of *pBR322* DNA plasmid in Tris–boric acid–EDTA buffer. Nuclease activities of both complexes were examined by gel electrophoresis, which allowed quantitative evaluation of different forms of the DNA. The percentage of total DNA cleavage was calculated by the following equation: DNA cleavage = $(D_{II} + 2 \times D_{III})/(D_I + D_{II} + 2 \times D_{III})$, where D_I, D_{II}, D_{III}: integrated density of SC-form, NC-form and LC-form respectively and shown in Tables S1–S3 in Supporting information [23]. It is clear from Fig. 4 that complex **1** alone exhibits a significant cleavage and single strand cleavage was enhanced as the complex concentration was increased (15–100 μM) (Fig. 4(A), lane 2–8) (50.4%, total DNA cleavage with 100 μM complex concentration, Table S1 in Supporting information). On the other hand, anhydrous $FeCl_3$ did not cleave plasmid DNA (Fig. 4(A), lane 2) at all. The oxidative DNA cleavage behaviour of the complex **1** was shown by combination of **1** (50 μM) and H_2O_2 (150–200 μM) resulted single strand scission (Fig. 4(B), lane 6) and double strand scission (Fig. 4(B), lanes 7–8) (~75%, total DNA cleavage, Table S2 in Supporting information) however, Kurosaki and co-workers [59] reported double strand cleavage of Fe(III)-BLM (0.1 mM) analogues with very high concentration of H_2O_2 (3 mM). Similar behaviour was observed for BME (10–100 μM) (Fig. 4(C), lane 3–6) with increase in BME concentration strand scission increased (SC form to NC and LC form) (~80%, total DNA cleavage, Table S3 in Supporting information).

Complex **2** was cleavage inactive in the presence oxidising (H_2O_2) or reducing agents (BME). No nuclease was appeared even in high concentration of BME (3 mM) (Fig. S4 in Supporting information). Mechanistic aspects of activity of nuclease of complex **1** was studied using different quenchers: singlet oxygen scavengers like NaN_3 or L-histidine and hydroxyl radical scavengers like DMSO, KI, urea, ethanol, D_2O. To check the mechanism of DNA cleavage activity via hydrolytic pathway we perform the experiment in presence of complex **1** and radical scavengers (Fig. S5 in Supporting information) nuclease activity was not inhibited by radical scavengers showing that only complex **1** could not generated reactive oxygen species (ROS) which were responsible for nuclease activity and exclude the possibility through hydrolytic pathway [46]. In case of oxidative cleavage, efficient inhibition was observed in presence of KI (Fig. 5, lane: 3) and small inhibitory effect was also found in presence of DMSO (Fig. 5, lane: 4). Inhibition in presence of KI and DMSO suggested the possibility of the formation of **.**OH radicals as the reactive species from probable hydroperoxo intermediate: $[Fe^{III}–OOH] \rightarrow [Fe^{IV} = O] + \mathbf{.}OH$. Similar result was reported by Chakravarty et al. with synthetic model for the bleomycins $[Fe(L')(L'')](PF_6)_3$ [31].

3.7. Detection of reactive oxygen species (ROS)

Reactive oxygen species in the cleavage reaction was detected by rhodamine B dye degradation [47] or by using sensitive radical sensor 1,3-diphenylisobenzofuran (DPBF) [48]. Participation of $OH^{\cdot}$ radicals or singlet oxygen ($^1O_2$) generation was also evaluated by rhodamine B dye and DPBF respectively, in presence of complexes **1** and **2**.

We have observed the decrease in absorbance of dye at 544 nm with increasing concentration of complex **1** (Fig. 6) however, there is no or slight change in absorbance of dye at 544 nm with increasing concentration of complex **2** (Fig. 6). These observations suggested the formation of $OH^{\cdot}$ radical in presence of **1**, which is probably responsible for degradation of dye. Generally, rhodamine B was oxidized by $OH^{\cdot}$ radical to yield a photo inactive rhodamine B adducts [63]. 1,3-diphenylisobenzofuran (DPBF) is the most well known $^1O_2$ acceptor and its emission is quenched in presence of $^1O_2$. In our experiment, DPBF was incubated with both complexes **1** and **2** and fluorescence at 479 nm (λ_{em} = 405 nm) is monitored. We observed slight quenching in fluorescence spectra of DPBF in

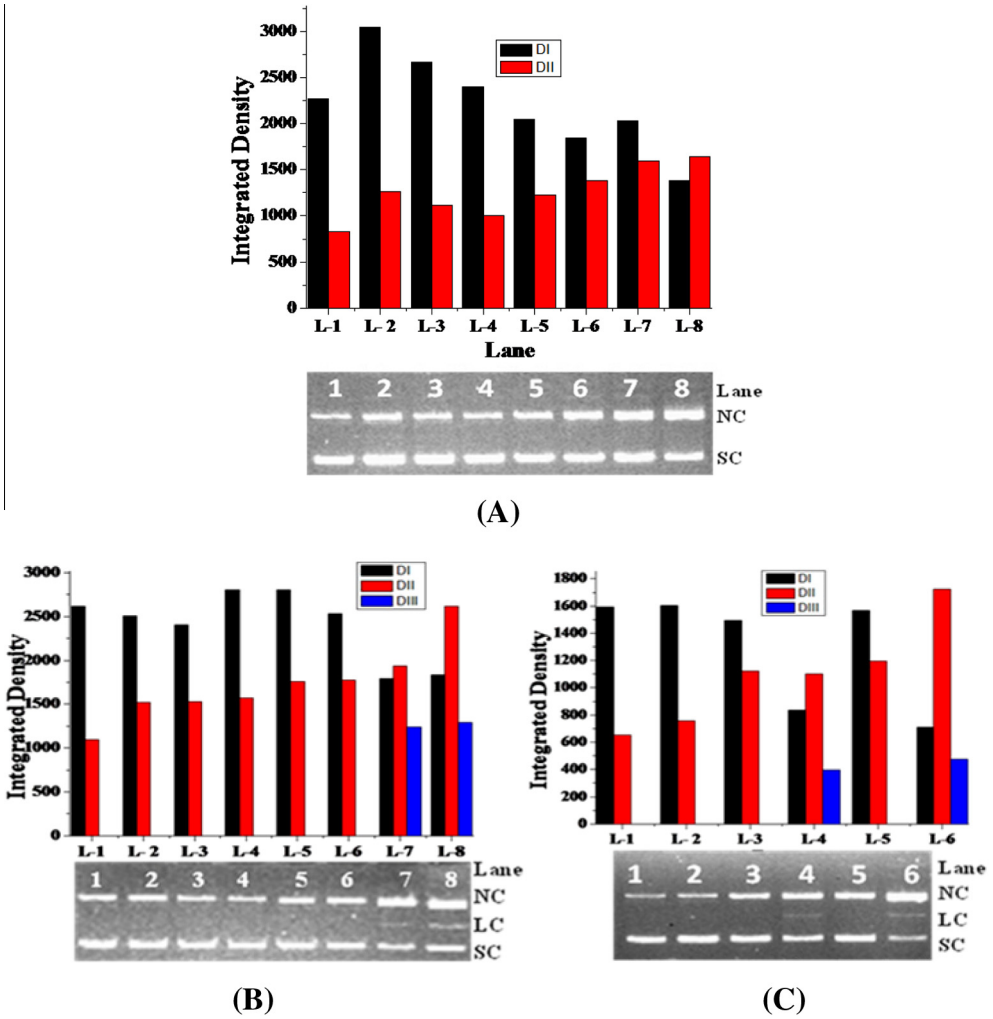

Fig. 4. Gel electrophoresis separations showing cleavage of supercoiled *pBR322* DNA (50 ng) by complex **1** in 10% dimethylformamide incubated at 37 °C for 3 h. (A) lane 1: DNA, lane 2: DNA + $FeCl_3$ (100 μM), lane 3: DNA + **1** (15 μM), lane 4: DNA + **1** (25 μM), lane 5: DNA + **1** (35 μM), lane 6: DNA + **1** (50 μM), lane 7: DNA + **1** (75 μM), lane 8: DNA + **1** (100 μM). (B) lane 1: DNA, lane 2: DNA + H_2O_2 (200 μM), lane 3: DNA + **1** (25 μM), Lane 4: DNA + **1** (25 μM) + H_2O_2 (25 μM), lane 5: DNA + **1** (25 μM) + H_2O_2 (50 μM), lane 6: DNA + **1** (25 μM) + H_2O_2 (100 μM), lane 7: DNA + **1** (50 μM) + H_2O_2 (150 μM), lane 8: DNA + **1** (50 μM) + H_2O_2 (200 μM). **(C)** lane 1: DNA, lane 2: DNA + BME (100 μM), lane 3: DNA + **1** (25 μM) + BME (10 μM), lane 4: DNA + **1** (25 μM) + BME (25 μM), lane 5: DNA + **1** (25 μM) + BME (50 μM), lane 6: DNA + **1** (25 μM) + BME (100 μM).

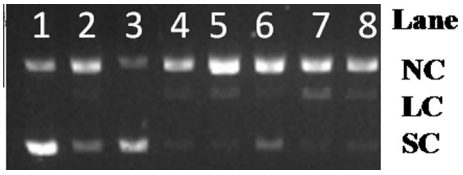

Fig. 5. Gel electrophoresis separations showing cleavage of supercoiled *pBR322* DNA (60 ng) by complex **1** in 10% dimethylformamide incubated at 37 °C for 3 h. lane 1: DNA, lane 2: DNA + **1** (15 μM) + H_2O_2 (100 μM), lane 3: DNA + **1** (15 μM) + H_2O_2 (100 μM) + KI (50 mM), lane 4: DNA + **1** (15 μM) + H_2O_2 (100 μM) + DMSO (100 mM), lane 5: DNA + **1** (15 μM) + H_2O_2 (100 μM) + Urea (100 mM), lane 6: DNA + **1** (15 μM) + H_2O_2 (100 μM) + NaN_3 (100 mM), lane 7: DNA + **1** (15 μM) + H_2O_2 (100 μM) + L-his (100 mM), lane 8: DNA + **1** (15 μM) + H_2O_2 (100 μM) + D_2O (100 mM).

presence of complexes **1** and **2** (Fig. S6 in Supporting information). These data indicated that $^1O_2$ was not produced the reaction mixture in presence of **1** or **2** [47].

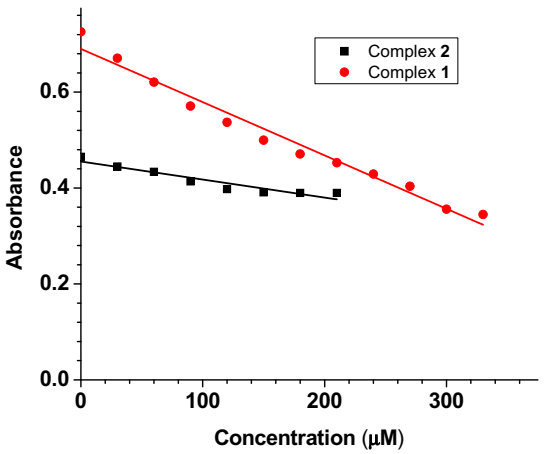

Fig. 6. Plot of decrease in absorbance of rhodamine B dye (5 μM) at 544 nm vs increasing concentration of metal complexes **1**, **2** (0–300 μM).

4. Conclusion

In the present work, we synthesised two mononuclear iron(III) complexes derived from a tridentate amidate ligand PampH, $[Fe(Pamp)(MeOH)Cl_2]$, **1** and $[Fe(Pamp)_2](ClO_4)$, **2**. Complexes **1** and **2** were characterized by conductivity measurements, IR and

UV–Vis spectral studies. Magnetic moments supported two different spin states namely high-spin state for **1** and low-spin state for **2**. Molecular structure of complex $[Fe(Pamp)_2](ClO_4)$, **2** was determined by single crystal X-ray crystallography. The stereochemistry around metal centre was described as distorted octahedral with two meridional spanning $Pamp^-$ ligands. DNA interaction studies obtained by fluorescence and circular dichroism spectral studies suggested external interaction with CT-DNA. Complex **1** exhibited good nuclease activity and mechanistic investigation shown probable participation of $OH^{\cdot}$ radical, which was trapped by reactive oxygen species (ROS) radical scavenger rhodamine B. Based on our results, complex **1** may initiate DNA cleavage in an oxidative manner.

Acknowledgements

K.G. is thankful to DST, New Delhi, India, for financial support (File No. SR/S1/IC-47/2012). N.T. and P.K. are thankful to CSIR, India, for financial assistance. UPS is thankful to IIT Roorkee for single crystal X-ray facility. We are thankful to Rajan Kumar for his help.

Appendix A. Supplementary material

Supplementary data associated with this article can be found, in the online version, at http://dx.doi.org/10.1016/j.ica.2013.11.034.

References

[1] K.E. Erkkila, D.T. Odom, J.K. Barton, Chem. Rev. 99 (1999) 2777.
[2] W.K. Pogozelski, T.D. Tullius, Chem. Rev. 98 (1998) 1089.
[3] M. Roy, R. Santhanagopal, A.R. Chakravarty, Dalton Trans. (2009) 1024.
[4] S.J. Lippard, Biochemistry 42 (2003) 2664.
[5] J. Reedijk, J. Inorg. Biochem. 86 (2001) 89.
[6] S.E. Wolkenberg, D.L. Boger, Chem. Rev. 102 (2002) 2477.
[7] B. Rosenberg, L. VanCamp, J.E. Trosko, V.H. Mansour, Nature 222 (1969) 385.
[8] E.R. Jamieson, S.J. Lippard, Chem. Rev. 99 (1999) 2467.
[9] R.M. Burger, Chem. Rev. 98 (1998) 1153.
[10] E. Wong, C.M. Giandomenico, Chem. Rev. 99 (1999) 2451.
[11] F.A. Cotton, G. Wilkinson, Advanced Inorganic Chemistry, fourth ed., Wiley, New York, 1980.
[12] C.D. Kaplan, J. Kaplan, Chem. Rev. 109 (2009) 4536.
[13] J.C. Joyner, J. Reichfield, J.A. Cowan, J. Am. Chem. Soc. 133 (2011) 15613.
[14] R.P. Megens, T.A. van den Berg, A.D. de Bruijn, B.L. Feringa, G. Roelfes, Chem. Eur. J. 15 (2009) 1723.
[15] X. Chen, J. Wang, S. Sun, J. Fan, S. Wu, J. Liu, S. Ma, L. Zhang, X. Peng, Bioorg. Med. Chem. Lett. 18 (2008) 109.
[16] X. Chen, J. Fan, X. Peng, J. Wang, S. Sun, R. Zhang, T. Wu, F. Zhang, J. Liu, F. Wang, S. Ma, Bioorg. Med. Chem. Lett. 19 (2009) 4139.
[17] X.Q. Chen, J.Y. Wang, T.Y. Zhang, L.Z. Zhang, X.J. Peng, Chin. Chem. Lett. 19 (2008) 342.
[18] C. Lu, S. Yu, D. Li, Z. Liao, Inorg. Chem. 41 (2002) 913.
[19] H. Kurosaki, A. Maruyama, H. Koike, N. Kuroda, Y. Ishikawa, M. Goto, Bioorg. Med. Chem. Lett. 12 (2002) 201.
[20] G.L. Parrilha, C. Fernandes, A.J. Bortoluzzi, B. Szpoganicz, Inorg. Chem. Commun. 11 (2008) 643.
[21] A. Neves, H. Terenzi, R. Horner, A. Horn Jr., B. Szpoganicz, J. Sugai, Inorg. Chem. Commun. 4 (2001) 388.
[22] A. Horn Jr., I. Vencato, A.J. Bortoluzzi, R. Horner, R.A.N. Silva, B. Spoganicz, V. Drago, H. Terenzi, M.C.B.D. Oliveira, R. Werner, W. Haase, A. Neves, Inorg. Chim. Acta 358 (2005) 339.
[23] R. Herchel, Z. Sindelar, Z. Travnicek, R. Zboril, J. Vanco, Dalton Trans. (2009) 9870.
[24] J. Qian, J.-L. Tian, L. Feng, W. Gu, X.-J. Zhao, S.-P. Yan, J. Coord. Chem. 62 (2009) 3276.
[25] L.M.T. Schnaith, R.S. Hanson, L. Que Jr., Proc. Natl. Acad. Sci. USA 91 (1994) 569.
[26] X.-Q. Chen, X.-J. Peng, J.-Y. Wang, Y. Wang, S. Wu, L.-Z. Zhang, T. Wu, Y.-K. Wu, Eur. J. Inorg. Chem. (2007) 5400.
[27] G.A. Woldemariam, S.S. Mandal, J. Inorg. Biochem. 102 (2008) 740.
[28] K.I. Ansari, J.D. Grant, G.A. Woldemariam, S. Kasiri, S.S. Mandal, Org. Biomol. Chem. 7 (2009) 926.
[29] S. Routier, H. Vezin, E. Lamour, J.-L. Bernier, J.-P. Catteau, C. Bailly, Nucleic Acid Res. 27 (1999) 4160.
[30] G. Roelfes, M.E. Branum, L. Wang, L. Que Jr., B.L. Feringa, J. Am. Chem. Soc. 122 (2000) 11517.
[31] A. Mukherjee, S. Dhar, M. Nethaji, A.R. Chakravarty, Dalton Trans. (2005) 349.
[32] Y.-L. Wong, C.-Y. Mak, H.S. Kwan, H.K. Lee, Inorg. Chim. Acta 363 (2010) 1246.
[33] R.K. Afshar, R. Bhalla, J.M. Rowland, M.M. Olmstead, P.K. Mascharak, Inorg. Chim. Acta 359 (2006) 4105.
[34] R.M. Burger, Struct. Bonding 97 (2000) 287.
[35] W. Huang, J. Jia, J. Cummings, M. Nelson, G. Schneider, Y. Lindqvist, Structure 5 (1997) 691.
[36] S. Zhu, W.W. Brennessel, R.G. Harrison, L. Que Jr., Inorg. Chim. Acta 337 (2002) 32.
[37] (a) R.K. Afshar, K.E. Granados, M.M. Olmstead, P.K. Mascharak, Inorg. Chem. Commun. 9 (2006) 1286. and references therein;
(b) R.J. Motekaitis, A.E. Martell, J. Am. Chem. Soc. 92 (1970) 4223.
[38] X. Tao, D.W. Stephan, P.K. Mascharak, Inorg. Chem. 26 (1987) 754.
[39] K. Ghosh, N. Tyagi, P. Kumar, Inorg. Chem. Commun. 13 (2010) 380.
[40] K. Ghosh, N. Tyagi, P. Kumar, S. Rathi, Inorg. Chem. Commun. 20 (2012) 167.
[41] K. Ghosh, N. Tyagi, P. Kamar, U.P. Singh, N. Goel, J. Inorg. Biochem. 104 (2010) 9.
[42] R.L. Dutta, A. Syamal, Elements of Magnetochemistry, second ed., Affiliated East-West Press, New Delhi, 1993. 8.
[43] G.M. Sheldrick, Acta Crystallogr., Sect. A 46 (1990) 467.
[44] G.M. Sheldrick, SHELXTL-NT 2000 Version 6.12, Reference Manual, University of Gottingen, Pergamon, New York, 1980.
[45] B. Klaus, University of Bonn, Germany DIAMOND, Version 1.2c, (1999).
[46] K. Ghosh, P. Kumar, N. Tyagi, Inorg. Chim. Acta 375 (2011) 77.
[47] S.S. Tonde, A.S. Kumbhar, S.B. Pandhye, R.J. Butcher, J. Inorg. Biochem. 100 (2006) 51.
[48] H.J. Yu, S.M. Huang, L.Y. Li, H.N. Jia, H. Chao, Z.W. Mao, J.Z. Liu, L.N. Ji, J. Inorg. Biochem. 103 (2009) 881.
[49] J.M. Rowland, M.M. Olmstead, P.K. Mascharak, Inorg. Chem. 41 (2002) 2754.
[50] C.M. Che, W.H. Leung, C.K. Li, H.Y. Cheng, S.M. Peng, Inorg. Chim. Acta 196 (1992) 43.
[51] J.M. Rowland, M. Olmstead, P.K. Mascharak, Inorg. Chem. 40 (2001) 2810.
[52] Y. Zang, J. Kim, Y. Dong, E.C. Wilkinson, E.H. Appelman, L. Que Jr., J. Am. Chem. Soc. 119 (1997) 4197.
[53] S. Wocadlo, W. Massa, J.-V. Folgado, Inorg. Chim. Acta 207 (1993) 199.
[54] P. Paul, B. Tyagi, M.M. Bhadbhade, E. Suresh, J. Chem. Soc., Dalton Trans. (1997) 2273.
[55] K. Nakamoto, Infrared and raman spectra of inorganic and coordination compounds, Part B, fifth ed., John Wiley & Sons, New York, 1997.
[56] M. Pascaly, C. Nazikkol, F. Schweppe, A. Wiedemann, K. Zurlinden, B. Krebs, Z. Anorg. Allg. Chem. 626 (2000) 50.
[57] A.K. Patra, M.M. Olmstead, P.K. Mascharak, Inorg. Chem. 41 (2002) 5403.
[58] K. Ghosh, P. Kumar, N. Tyagi, U.P. Singh, V. Aggarwal, M.C. Baratto, Eur. J. Med. Chem. 45 (2010) 3770.
[59] H. Kurosaki, Y. Ishikawa, K. Hayashi, M. Sumi, Y. Tanaka, M. Goto, K. Inada, I. Taniguchi, M. Shionoya, H. Matsuo, M. Sugiyama, E. Kimura, Inorg. Chim. Acta 294 (1999) 56.
[60] J.C.A. Boeyens, A.G.S. Forbes, R.D. Hancock, K. Wieghardt, Inorg. Chem. 24 (1985) 2926.
[61] Z.-D. Xu, H. Liu, M. Wang, S.-L. Xiao, M. Yang, X.-H. Bu, J. Inorg. Biochem. 92 (2002) 149.
[62] Z.-D. Xu, H. Liu, S.-L. Xiao, M. Yang, X.-H. Bu, J. Inorg. Biochem. 90 (2002) 79.
[63] F. Yu, D. Xu, R. Lei, N. Li, K. Li, J. Agric. Food Chem. 56 (2008) 730.